NeuroImage: Clinical 14 (2017) 610–621

Contents lists available at ScienceDirect

NeuroImage: Clinical

journal homepage: www.elsevier.com/locate/ynicl

Radiation-induced abnormal cortical thickness in patients with nasopharyngeal carcinoma after radiotherapy

Jiabao Lin[a,1], Xiaofei Lv[b,1], Meiqi Niu[a], Lizhi Liu[b], Jun Chen[a], Fei Xie[b], Miao Zhong[a], Shijun Qiu[c], Li Li[b,*], Ruiwang Huang[a,**]

[a] Center for the Study of Applied Psychology, Guangdong Key Laboratory of Mental Health and Cognitive Science, School of Psychology, South China Normal University, Guangzhou 510631, PR China
[b] Department of Medical Imaging, Collaborative Innovation Centre for Cancer Medicine, State Key Laboratory of Oncology in South China, Sun Yat-sen University Cancer Centre, Guangzhou 510060, PR China
[c] Department of Medical Imaging, The First Affiliated Hospital of Guangzhou University of Chinese Traditional Medicine, Guangzhou 510405, PR China

ARTICLE INFO

Article history:
Received 18 September 2016
Received in revised form 2 February 2017
Accepted 28 February 2017
Available online 2 March 2017

Keywords:
Structural MRI
Brain injury
Cortical thickness
Radiotherapy
Surface-based morphometry

ABSTRACT

Conventional MRI studies showed that radiation-induced brain necrosis in patients with nasopharyngeal carcinoma (NPC) in years after radiotherapy (RT) could involve brain gray matter (GM) and impair brain function. However, it is still unclear the radiation-induced brain morphological changes in NPC patients with normal-appearing GM in the early period after RT. In this study, we acquired high-resolution brain structural MRI data from three groups of patients, 22 before radiotherapy (pre-RT) NPC patients with newly diagnosed but not yet medically treated, 22 NPC patients in the early-delayed stage after radiotherapy (post-RT-ED), and 20 NPC patients in the late-delayed stage after radiotherapy (post-RT-LD), and then analyzed the radiation-induced cortical thickness alteration in NPC patients after RT. Using a vertex-wise surface-based morphometry (SBM) approach, we detected significantly decreased cortical thickness in the precentral gyrus (PreCG) in the post-RT-ED group compared to the pre-RT group. And the post-RT-LD group showed significantly increased cortical thickness in widespread brain regions, including the bilateral inferior parietal, left isthmus of the cingulate, left bank of the superior temporal sulcus and left lateral occipital regions, compared to the pre-RT group, and in the bilateral PreCG compared to the post-RT-ED group. Similar analysis with ROI-wise SBM method also found the consistent results. These results indicated that radiation-induced brain injury mainly occurred in the post-RT-LD group and the cortical thickness alterations after RT were dynamic in different periods. Our findings may reflect the pathogenesis of radiation-induced brain injury in NPC patients with normal-appearing GM and an early intervention is necessary for protecting GM during RT.

1. Introduction

Radiation-induced brain injury, including structural and functional deficits, is a severe complication for patients with nasopharyngeal carcinoma (NPC) after radiotherapy (RT) (Zeng, et al., 2015). Based on the onset time of RT, three phases of the pathophysiological reaction to irradiation in normal brain tissue can be classified, acute reaction period (few days to few weeks), early delayed radiation period (1–6 months), and late delayed radiation period (6 months to few years) (Lell, 2015). Previous studies mainly focused on the radiation-induced functional deficits and structural necrosis (irreversible and progressive) in NPC patients in the late-delayed period after RT (Hsiao, et al., 2010; Shen, et al., 2015). However, most NPC patients after RT exhibited little change in their brain tissue according to the routine conventional MRI examination (Wang, et al., 2012), but they had the potential to suffer the radiation-induced cognitive impairment in future (Hsiao, et al., 2010). Thus, it is necessary to evaluate early radiation-induced injury (potentially reversible) in the NPC patients with normal-appearing brain tissue and

Abbreviations: NPC, nasopharyngeal carcinoma; RT, radiotherapy; GM, gray matter; pre-RT, before radiotherapy; post-RT-ED, in the early-delayed stage after radiotherapy; post-RT-LD, in the late-delayed stage after radiotherapy; SBM, surface-based morphometry; CMBs, cerebral microbleeds; WM, white matter; VBM, voxel-based morphometry; AJCC, American Joint Committee on Cancer; 2D-CRT, conventional two-dimensional radiotherapy; IMRT, intensity-modulated radiation therapy; KPS, Karnofsky performance status scale; FWHM, full width at half maximum; ANOVA, analysis of variance; GLM, general linear model; FDR, false discovery rate; CT, cortical thickness; RA, relative alteration; PreCG, precentral gyrus; bSTS, bank of the superior temporal sulcus; ICC, isthmus of the cingulate cortex; LOC, lateral occipital cortex; IPC, inferior parietal cortex; PoCG, postcentral gyrus; cMFC, caudal middle frontal cortex; STC, superior temporal cortex; MTC, middle temporal cortex; PreCUN, precuneus; DMN, default mode network.

* Correspondence to: L. Li, State Key Laboratory of Oncology in South China, Sun Yat-sen University Cancer Centre, 651 Dongfeng East Road, Guangzhou 510060, PR China.
** Correspondence to: R. Huang, School of Psychology, South China Normal University, Guangzhou 510631, PR China.
E-mail addresses: li2@mail.sysu.edu.cn (L. Li), ruiwang.huang@gmail.com (R. Huang).
[1] These authors contributed equally to this work.

http://dx.doi.org/10.1016/j.nicl.2017.02.025

then provide neuroimaging biomarkers to facilitate clinical diagnose, treatment, and prevention.

Several underlying pathophysiological mechanisms have been described as cerebral microbleeds (CMBs), white matter (WM) and gray matter (GM) lesions in NPC patients after RT (Chan, et al., 1999; Chen, et al., 2015; Shen, et al., 2015). And CMBs in the temporal lobe is believed associating with increased likelihood of cognitive dysfunctions in NPC patients after RT (Shen, et al., 2015). Previous studies have found WM alterations in the temporal lobe in the earlier period after RT, including metabolic changes (Xiong, et al., 2013), and abnormalities of water diffusion (Chen, et al., 2015). Actually, brain abnormalities after RT may be multifocal and dispersed throughout GM within the treatment fields (Peterson, et al., 1995), especially in the temporal lobe (Chan, et al., 1999). Studies indicated that radiation-induced GM necrosis are often found in years after the completion of RT and are predominant hyper-intense on the conventional MRI (Chan, et al., 1999; Peterson, et al., 1995). To date, it is still unclear the radiation-induced brain morphological changes in normal-appearing GM in NPC patients in the early period after RT. Thus, objective methods are needed to characterize it thoroughly.

Both voxel-based morphometry (VBM) and surface-based morphometry (SBM) analyses were widely used to examine the morphological GM changes in various diseases, such as leukemia (Tamnes, et al., 2015), breast cancer (de Ruiter, et al., 2012), and glioma (Karunamuni, et al., 2016). With VBM analysis, Lv, et al. (2014) examined the radiation-induced changes in normal-appearing GM for NPC patients and found GM volume deficits in the temporal lobe in patients after RT. However, the VBM approach has some limitations. The smoothing step, registration, and templates used in the VBM analysis might influence the accuracy of the results (Li, et al., 2014). On the other hand, the VBM analysis potentially confounded several parameters, including cortical thickness, cortical surface area, and cortical folding (Grant, et al., 2015). Therefore, the alternative approach of SBM analysis has been developed, which facilitates highly sensitive characterization of cortical thickness, and provides more sensitive measurements of GM compared to the GM volume measure used with VBM analysis (Li, et al., 2014; Pereira, et al., 2012).

In practice, both vertex-wise and ROI-wise SBM approaches are widely used to assess the abnormalities of cortical thickness in various brain diseases (Blanc, et al., 2015; Jednoróg, et al., 2012). For example, the vertex-wise SBM approach been used to characterize patterns of GM changes in Alzheimer's disease (Blanc, et al., 2015), Parkinson's disease (Biundo, et al., 2015), and Depressive disorder (Qiu, et al., 2014), while the ROI-wise SBM approach has been used to depict brain morphometry involving socioeconomic status on children's brain structures (Jednoróg, et al., 2012), childhood maltreatment on brain structures (Kelly, et al., 2013), and brain structures of individuals with high familial risk of mood disorders (Papmeyer, et al., 2015). However, as far as we know, no studies have reported radiation-induced cortical thickness abnormalities in the normal-appearing GM for NPC patients with SBM approach.

The present study aims to noninvasively measure the radiation-induced changes of cortical thickness in the normal-appearing GM in NPC patients before and in different periods after RT using both vertex- and ROI-wise SBM approaches. NPC is sensitive to the radiation and the bilateral temporal lobes in these patients receive high doses of radiation because the temporal lobes are near to the tumor (Chan, et al., 1999; Lell, 2015). Thus, these patients have the potential for development of radiation-induced damage to the temporal lobes. Previous studies (Khong, et al., 2006; Moretti, et al., 2005) reported that NPC patients who received RT showed profound alterations of frontal functions, such as attention focusing, executive functions, and analogical judgment. And functional impairment in vision was common found in NPC patients who received RT (Chen, et al., 2005; Fang, et al., 2002; Wang, et al., 2012). Considering the findings of these studies, we hypothesized that cortical thickness would be altered in some areas of the brain in NPC patients after RT, especially in the temporal, frontal and occipital regions.

2. Material and methods

2.1. Subjects

We recruited 64 patients (51 M/13 F, aged 22–63 years old, 46.06 ± 8.69 years old, Han Chinese population) who were diagnosed with nonkeratinizing undifferentiated NPC from the Sun Yat-sen University Cancer Center, Guangzhou, China. All patients were diagnosed on the basis of histopathology. The clinical stages of NPC were classified according to American Joint Committee (AJCC) on cancer staging system (7th edition) (Edge and Compton, 2010), and the TNM (T = Tumor, N = Nodes, and M = Metastasis) stage for all of the patients were ranged from T1N0M0 to T4N2M0. Each patient underwent a detailed pre-treatment evaluation, including physical examination, nasopharyngeal fiberoptic endoscopy, MRI scan of the nasopharynx and neck, chest radiography, abdominal sonography, and whole body bone scan. We divided the 64 patients into 2 subgroups according to the time before and after completion of RT. Among the patients, 22 were before radiotherapy (pre-RT) patients with staging from T1N0M0 to T4N2M0, while the remaining 42 were after radiotherapy (post-RT) patients with staging from T1N0M0 to T4N2M0. The duration period between the receiving RT and MRI scanning was in range of 1–18 months.

Based on the onset time of symptom, the typical brain response to RT has been divided into three periods, the acute reaction period (few days to few weeks), early delayed radiation period (1–6 months), and late delayed radiation period (6 months to few years) (Duan, et al., 2016; Moretti, et al., 2005; New, 2001). To explore the effect of RT on brain structure in different periods, we sub-classified all of the 42 post-RT patients in the present study into two groups. One group, the post-RT-ED group, included 22 patients in the early-delayed stage after RT who had undergone 1–6 months RT prior to the MRI scanning. And the other group, the post-RT-LD group, included 20 patients in the late-delayed stage after RT who had undergone 7–18 months RT prior to the MRI scanning. Fig. 1 illustrates the procedures for selecting NPC patients in this study.

The protocol for nasopharynx and neck RT included the conventional two-dimensional radiotherapy (2D-CRT) and intensity-modulated radiation therapy (IMRT). The description of the 2D-CRT and IMRT techniques used in the present study can be found in previous studies (Lai, et al., 2011; Sun, et al., 2013; Xia, et al., 2000). In the 2D-CRT treatment, patients were immobilized in the supine position with a mask and treated with two lateral opposing faciocervical portals to irradiate the nasopharynx and the upper neck in one volume, followed by application of the shrinking-field technique to limit irradiation of the spinal cord. An anterior cervical field was used to treat the neck with a laryngeal block. The accumulated radiation doses were 66–76 Gy with 2 Gy per fraction applied to the primary tumor for each patient. In the IMRT treatment, immobilization for IMRT was the same as that used for 2D-CRT, and the primary tumor and the upper neck above the caudal edge of the cricoid cartilage were treated with IMRT. Then inverse IMRT planning was performed using the Corvus system (version 3.0, Peacock, Nomos, Deer Park, IL, USA). Meanwhile, a MIMiC multileaf collimator (Nomos, Sewickley, PA, USA) was used for planning and treatment. The total dose of radiotherapy was 58–70 Gy, divided into 30–33 fractions. Moreover, for the patients with stage I to IIa disease, no chemotherapy was required according to the guidelines (defined by the 6th edition of the UICC/AJCC staging system for NPC). However, it was recommended to provide concurrent chemoradiotherapy for stage IIb, and concurrent chemoradiotherapy with/without neoadjuvant/adjuvant chemotherapy for stages III to IVa–b. Overall, 1 patient in the post-RT-ED group and 1 patient in the post-RT-LD group received only RT. The remaining patients were treated with concurrent chemoradiotherapy, with cisplatin and 5-FU and/or 1–3 courses of neoadjuvant/

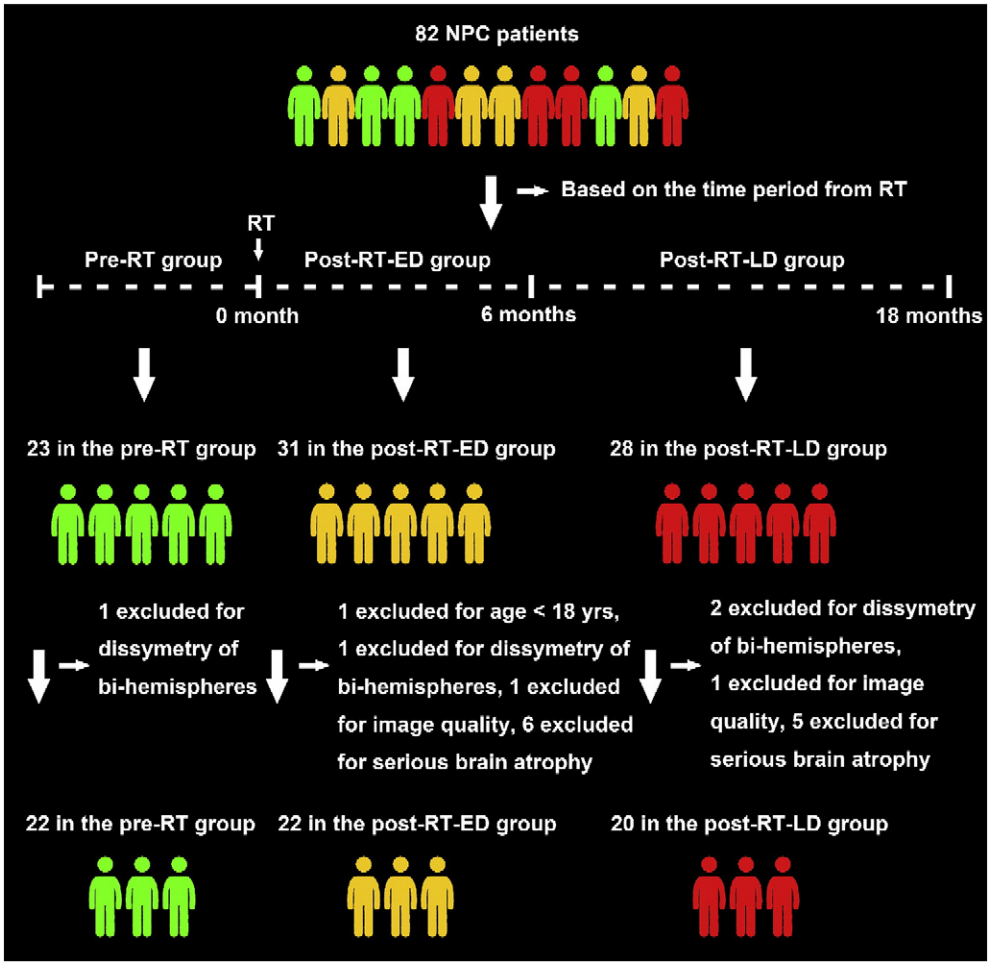

Fig. 1. The procedure for selecting patients with nasopharyngeal carcinoma in the before radiotherapy (pre-RT) group, after radiotherapy (post-RT-ED) group of the early-delayed stage, and after radiotherapy (post-RT-LD) group of the late-delayed stage in this study.

adjuvant chemotherapy 1–3 months before/after RT with one or more agents, such as cisplatin, docetaxel, 5-FU, and nedaplatin. For each NPC patients in the present study, the overall function was assessed according to the Karnofsky performance status (KPS) scale (Yates, et al., 1980).

Exclusion criteria for all patients in this study were as follows: intracranial invasion, brain tumors or metastases, alcoholism, neurological or psychiatric diseases, prior substantial head trauma, positive human immunodeficiency virus status, viral hepatitis, hypertension, diabetes, left-handed, other major medical illness, and contraindications for MRI scanning. The study protocol was approved by the Institutional Review Board of the Sun Yat-sen University Cancer Center. Written informed consent was obtained from each subject prior to the study. The demographic characteristics of the NPC patients are listed in Table 1.

Table 1
Demographic characteristics of the patients with nasopharyngeal carcinoma in the before radiotherapy (pre-RT) group, the after radiotherapy (post-RT-ED) group of the early-delayed stage, and the after radiotherapy (post-RT-LD) group of the late-delayed stage in this study. One-way analysis of variance (ANOVA) with Bonferroni post hoc tests was performed to assess differences in age, Karnofsky performance status (KPS) score, and total intracranial volume. And a χ^2-test was used to assess the differences in gender composition, AJCC stage among the three groups, and treatment protocol, chemotherapy between the post-RT-ED and post-RT-LD group ($p < 0.05$, two-sided). Abbreviations: N/A, not applicable; AJCC, American Joint Committee on Cancer; 2D–CRT, conventional two-dimensional radiotherapy; IMRT, intensity-modulated radiation therapy.

Characteristics	Pre-RT	Post-RT-ED	Post-RT-LD	*p*-Value
Age (years old)	44.09 ± 9.54	48.59 ± 5.96	45.45 ± 9.91	0.22
Gender (female/male)	5/17	3/19	5/15	0.62
Total intracranial volume (cm^3)	1437.32 ± 131.33	1477.81 ± 157.38	1480.48 ± 143.44	0.55
Karnofsky performance status (KPS) score	87.05 ± 3.72	86.77 ± 2.71	86.90 ± 2.92	0.96
Period between RT and imaging (months)	N/A	3.32 ± 1.59	10.90 ± 1.68	
Chemotherapy (with/without)	N/A	21/1	19/1	0.95
Treatment protocol (2D–CRT/IMRT)	N/A	18/4	13/7	0.22
AJCC stage (I/II/III/IV)	1/4/12/5	1/8/9/4	1/5/9/5	0.91

2.2. Data acquisition

All MRI data were acquired on a 3 T Siemens Trio Tim MRI scanner in the Department of Medical Imaging, Sun Yat-sen University Cancer Center. For each patient, the high-resolution brain structural images were obtained using a T1-weighted 3D magnetization prepared rapid acquisition gradient echo (MP-RAGE) sequence with the following parameters: repetition time (TR) = 1900 ms, echo time (TE) = 2.52 ms, inversion time (TI) = 900 ms, field of view (FOV) = 256 × 256 mm^2, flip angle (FA) = 9°, data matrix = 256 × 256, voxel size = 1.0 × 1.0 × 1.0 mm^3, 176 sagittal slices covering the whole brain. In addition, we also acquired the conventional T1-weighted, T2-weighted, and T2-FLAIR images as the routine data to detect any clinically brain lesions for each patient. Brain images for each patient were evaluated by two radiologists (X.L. and L.L.) specializing in diagnostic imaging of the central nervous system.

2.3. Data preprocessing

Cortical thickness was estimated with FreeSurfer package (version 5.3.0, http://surfer.nmr.mgh.harvard.edu), a set of automated programs used for cortical surface reconstruction and thickness measurement (Dale, et al., 1999; Fischl, et al., 1999). The reconstruction of the cortical surface consists of the following steps. First, an automated Talairach registration was performed and intensity variations due to magnetic field inhomogeneity were corrected. Second, a "skull-stripping" procedure was used to remove extra-cerebral voxels and to classify brain WM and GM automatically based on intensity and neighbor constraints. Cutting planes were also computed to separate the two hemispheres and to disconnect subcortical structures. Third, a tessellated mesh consisting of over 300,000 vertices was constructed over the WM surface and then deformed to produce an accurate and smooth representation of the GM/WM interface as well as the pial surface. In the calculations, we corrected topological 'defects' derived from brain segmentation by using a manual editing procedure if necessary. Fourth, at each vertex, the cortical thickness was calculated by averaging the shortest distance from a given point on the WM/GM surface to the pial surface and the shortest distance from the corresponding point on the pial surface to the WM/GM surface. The reconstructed surface was inflated and transformed to an average spherical surface with cortical folding patterns of the gyri and sulci normalized. At last, the cerebral cortex was automatically parcellated into standard gyral brain regions which was defined according to the Desikan-Killiany atlas or the Destrieux atlas and the average cortical thickness of each region was extracted. Cortical thickness measures were mapped on the spherical surface with a common spherical coordinate system. The cortical thickness was smoothed with a Gaussian kernel of 10-mm full width at half maximum (FWHM).

2.4. Statistical analyses

2.4.1. Subject characteristics

One-way analysis of variance (ANOVA) with Bonferroni post hoc tests was performed to assess the differences in age, KPS scale score, and total intracranial volume. And a χ^2-test was used to assess the differences in gender composition, AJCC stage among the three groups, and treatment protocol, chemotherapy between the post-RT-ED and post-RT-LD group. Statistical analyses were performed using SPSS software (version 19.0; SPSS, Chicago, IL, USA) and the significant level was set at $p < 0.05$ (two-sided).

2.4.2. Vertex-wise SBM analysis of cortical thickness

We first performed vertex-wise SBM analysis for each subject and then determined between-group differences in cortical thickness by using FreeSurfer Qdec (**q**uery, **d**esign, **e**stimate, and **c**ontrast) (http://surfer.nmr.mgh.harvard.edu/fswiki/Qdec). For each hemisphere, a general linear model (GLM) was used to compute vertex-wise between-group difference in cortical thickness. As previous studies suggested cortical thickness is easily influenced by gender and age (Giedd and Rapoport, 2010), we took gender and age as covariates to avoid spurious results while running the GLM. We separately estimated three between-group differences in cortical thickness, i.e., post-RT-ED vs. pre-RT groups, post-RT-LD vs. pre-RT groups, and post-RT-ED vs. post-RT-LD groups. Corrections for multiple comparisons across the whole brain were performed using the Monte Carlo permutation cluster analysis (10,000 iterations) and a cluster threshold of $p < 0.05$ (two-tailed). In this way, we determined the surviving clusters which were presented in this study.

2.4.3. ROI-wise SBM analysis of cortical thickness

We also performed an ROI-wise SBM analysis to supplement the findings of vertex-wise SBM analysis. The reason is that the vertex-wise SBM analysis is only performed on the vertex level but without considering brain specific sulco-gyral structure, which might pose discrepancies when we compare our results with previous studies (Li, et al., 2014). In the calculations, we adopted the Destrieux atlas to subdivide each hemisphere into 74 ROIs, which contain information about either gyral or sulci structures in the human brain, and thus a total 148 ROIs for the whole cortex (Destrieux, et al., 2010). For each ROI, the mean cortical thickness was extracted and a nonparametric permutation test was used to test significant between-group difference in cortical thickness (10,000 permutations). In the calculations, we also took gender and age as covariates. Multiple-comparison corrections were performed with a false discovery rate (FDR) at a threshold of $p < 0.05$ (two-tailed).

To assess the relationship between cortical thickness and time after RT, we first determined the ROIs showing significant between-group differences in cortical thickness, then estimated the averaged cortical thickness across all subjects for each group in these ROIs, and finally showed cortical thickness alterations of these ROIs across time after RT. In addition, to show the alterations in cortical thickness (*CT*) (*RA*) in *CT* for a given ROI using the following equations

$$\begin{aligned} RA_{\text{post-RT-ED}} &= \left(CT_{\text{post-RT-ED}} - CT_{\text{pre-RT}}\right)/CT_{\text{pre-RT}}, \\ RA_{\text{post-RT-LD}} &= \left(CT_{\text{post-RT-LD}} - CT_{\text{pre-RT}}\right)/CT_{\text{pre-RT}}, \\ RA_{\text{post-RT-LD}} &= \left(CT_{\text{post-RT-LD}} - CT_{\text{post-RT-ED}}\right)/CT_{\text{post-RT-ED}} \end{aligned} \quad (1)$$

where $CT_{\text{post-RT-LD}}$ ($CT_{\text{post-RT-ED}}$ and $CT_{\text{pre-RT}}$) represents the group averaged cortical thickness in the post-RT-LD (post-RT-ED and pre-RT) group for a given ROI. For each of the 148 ROIs in the Destrieux atlas, we estimated the *RA* in the *CT*.

3. Results

3.1. Subject characteristics

Table 1 lists the demographic and clinical characteristics of the three groups. No significant difference was found in age, gender, KPS scale scores, total intracranial volume and AJCC stage among the three groups. And no significant difference was found in either treatment protocol or chemotherapy between the post-RT-ED and post-RT-LD group.

3.2. Vertex-wise SBM analysis of cortical thickness

Pre-RT vs. *post-RT-ED*: Vertex-wise SBM analysis showed only one cluster with significantly decreased cortical thickness in the post-RT-ED group compared to the pre-RT group ($p = 0.0421$, corrected), which is presented in Fig. 2. This cluster (referred as C1) is located in the left precentral gyrus (PreCG) (Table 2). No other clusters were detected showing significant between-group difference in cortical thickness after multiple-comparison corrections.

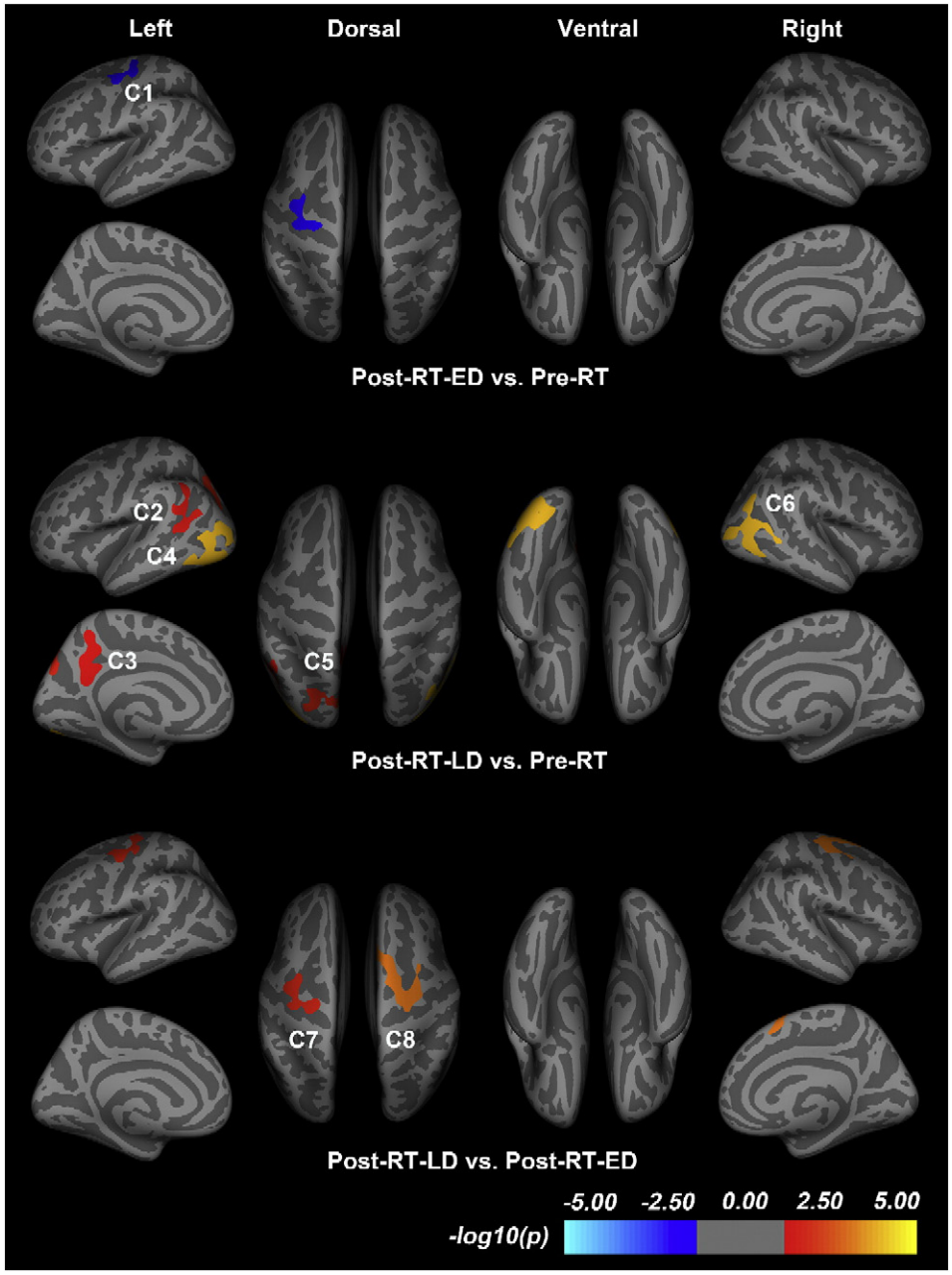

Fig. 2. Vertex-wise comparison of cortical thickness in the patients with nasopharyngeal carcinoma in the before radiotherapy (pre-RT) group, the after radiotherapy (post-RT-ED) group of the early-delayed stage, and the after radiotherapy (post-RT-LD) group of the late-delayed stage in this study. The clusters correspond to the regions with statistically significant group difference in cortical thickness. In the calculations, we used Monte Carlo simulation, with a threshold of $p < 0.05$, to provide cluster-wise multiple-testing comparisons. The color bar indicates the significance level of group differences. Clusters in cold (warm) color indicate significantly decreased (increased) cortical thickness in the post-RT-ED (post-RT-LD) compared to pre-RT (pre-RT or post-RT-ED) group. Details of these clusters are listed in Table 2.

Pre-RT vs. *post-RT-LD*: Fig. 2 shows the five clusters with uniformly significantly increased cortical thickness in the post-RT-LD group compared to the pre-RT group (Table 2). Four clusters in the left hemisphere are mainly located in bank of the superior temporal sulcus (bSTS, referred as C2) ($p = 0.0250$, corrected), isthmus of the cingulate cortex (ICC, C3) ($p = 0.0318$, corrected), lateral occipital cortex (LOC, C4) ($p = 0.0001$, corrected), and inferior parietal cortex (IPC, C5) ($p = 0.0146$, corrected). While the other one in the right hemisphere is located in the inferior parietal cortex (IPC, C6) ($p = 0.0001$, corrected).

Post-RT-ED vs. *post-RT-LD:* We found two clusters showing uniformly significantly increased cortical thickness in the post-RT-LD group compared to the post-RT-ED group (Fig. 2 and Table 2). One cluster is mainly located in the left precentral gyrus (PreCG, C7) ($p = 0.0136$, corrected), while the other cluster in the right precentral gyrus (PreCG, C8) ($p = 0.0008$, corrected).

3.3. ROI-wise SBM analysis of cortical thickness

3.3.1. Pre-RT vs. post-RT-ED

For all the 148 ROIs derived from Destrieux atlas, we found no ROI showing significantly changed cortical thickness in the post-RT-ED group compared to the pre-RT group.

3.3.2. Pre-RT vs. post-RT-LD

For the 148 ROIs of Destrieux atlas, we found 22 ROIs which had uniformly significantly increased cortical thickness in the post-RT-LD group

Table 2
Cortical clusters showing significant differences in cortical thickness between the patients with nasopharyngeal carcinoma in the before radiotherapy (pre-RT) group, after radiotherapy (post-RT-ED) group of the early-delayed stage, and the after radiotherapy group (post-RT-LD) of the late-delayed stage in this study. Clusters were obtained using Monte Carlo simulation with a threshold of $p < 0.05$, to provide cluster-wise correction for multiple comparisons. The cluster-wise p-value corresponds to the peak vertex showing greatest statistical difference within a cluster. Abbreviations: PreCG, precentral gyrus; PoCG, postcentral gyrus; cMFC, caudal middle frontal cortex; bSTS, bank of the superior temporal sulcus; MTC, middle temporal cortex; STC, superior temporal cortex; IPC, inferior parietal cortex; SMG, supramarginal gyrus; ICC, isthmus of the cingulate cortex; PreCUN, precuneus; LOC, lateral occipital cortex; ITC, inferior temporal cortex; FFG, fusiform gyrus; LING, lingual gyrus; SPC, superior parietal cortex; CUN, cuneus; SFC, superior frontal cortex.

Between-group comparison	Index	Location	Cluster size (mm^2)	No. of vertices	Peak Talairach Coordinates			p-Value ($\times 10^{-3}$)
					x	*y*	*z*	
Post-RT-ED < Pre-RT	C1	PreCG.L, PoCG.L, cMFC.L	832.7	1929	−32.6	−24.2	44.6	42.1
Post-RT-LD > Pre-RT	C2	bSTS.L, MTC.L, STC.L, IPC.L, SMG.L	902.4	1985	−45.1	−52.3	9.6	25.0
	C3	ICC.L, PreCUN.L	868.2	1868	−8.3	−48.7	26.6	31.8
	C4	LOC.L, ITC.L, MTC.L, FFG.L, IPC.L, LING.L	2433.8	3673	−40.2	−71	7.6	0.1
	C5	IPC.L, SPC.L, PreCUN.L, CUN.L	976.7	1788	−30.9	−74.5	17.8	14.6
	C6	IPC.R, ITC.R, MTC.R, LOC.R	1750.4	2732	45.2	−67.6	12.3	0.1
Post-RT-LD > Post-RT-ED	C7	PreCG.L, PoCG.L, cMFC.L	991.7	2302	−38.4	−5.1	52.2	13.6
	C8	PreCG.R, cMFC.R, SFC.R	1468.6	3083	26.7	−10.9	62.5	0.80

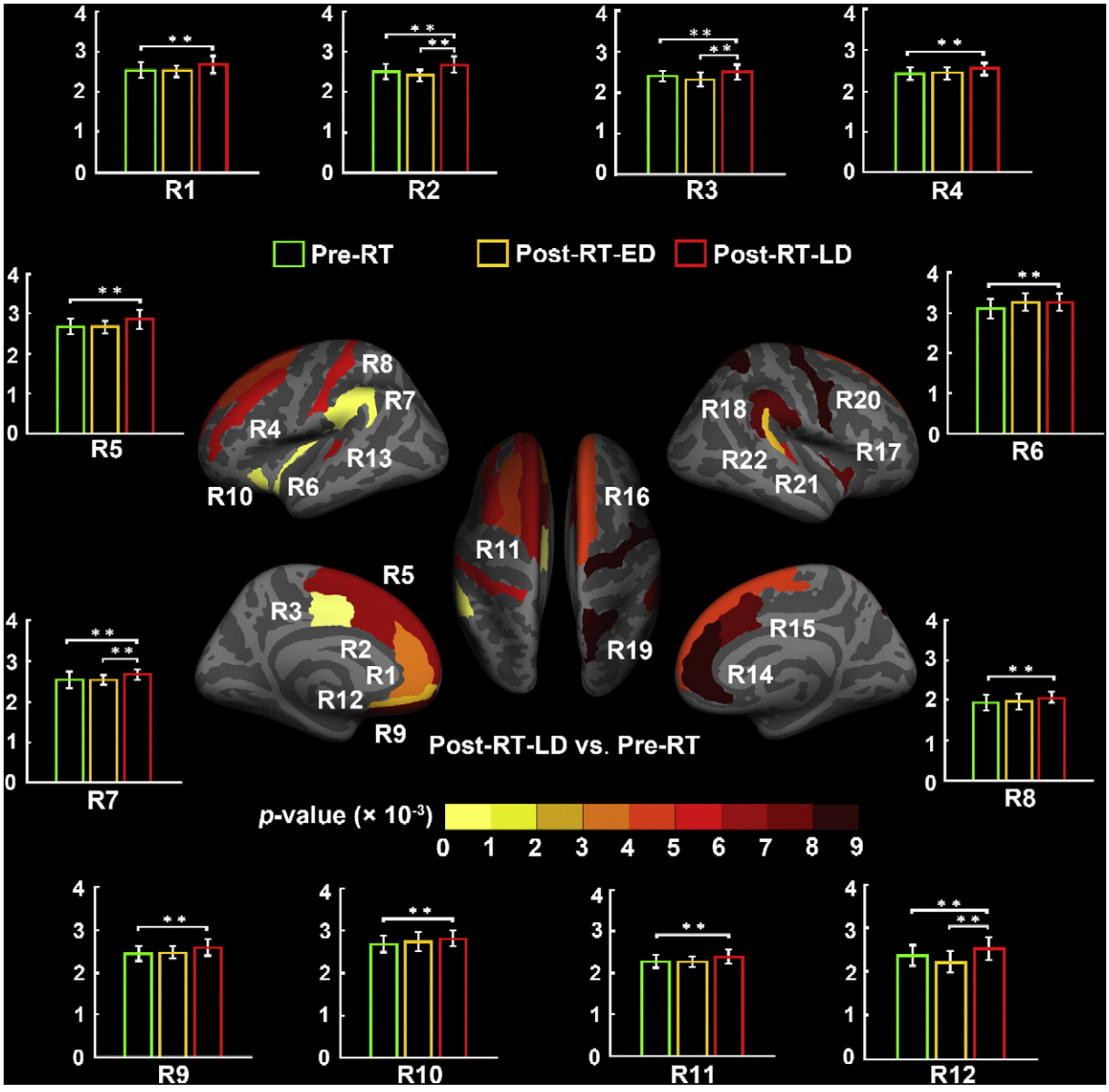

Fig. 3. ROI-wise analysis of cortical thickness between the patients with nasopharyngeal carcinoma in the before radiotherapy (pre-RT) group and the after radiotherapy (post-RT-LD) group of the late-delayed stage in this study. This analysis was based on each region of the Destrieux cortical atlas which parcellates each hemisphere into 74 ROIs. Specifically, 22 of the total 148 brain regions in warm color show significantly increased thickness in the post-RT-LD group compared to the pre-RT group. Details of cortical thickness for these ROIs are listed in Table 3.

Table 3
Brain regions showing significantly altered cortical thickness (*CT*) between the patients with nasopharyngeal carcinoma in the before radiotherapy (pre-RT) group, the after radiotherapy (post-RT-ED) group of the early-delayed stage, and the after radiotherapy group (post-RT-LD) of the late-delayed stage in this study. Brain regions were extracted from the Destrieux cortical atlas which contains 74 regions for each hemisphere. The significant group differences in cortical thickness in each region were determined at a threshold of $p < 0.05$ with a false discovery rate (FDR) multiple-testing correction. For a given region, we estimated the relative alteration (*RA*) in *CT* by using the following equations: $RA_{\text{post-RT-ED}} = (CT_{\text{post-RT-ED}}\text{-}CT_{\text{pre-RT}}) / CT_{\text{pre-RT}}$, $RA_{\text{post-RT-LD}} = (CT_{\text{post-RT-LD}}\text{-}CT_{\text{pre-RT}}) / CT_{\text{pre-RT}}$, and $RA_{\text{post-RT-LD}} = (CT_{\text{post-RT-LD}}\text{-}CT_{\text{post-RT-ED}}) / CT_{\text{post-RT-ED}}$. Abbreviations: G_and_S_cingul-Ant, anterior part of the cingulate gyrus and sulcus; G_and_S_cingul-Mid-Ant, middle-anterior part of the cingulate gyrus and sulcus; G_and_S_cingul-Mid-Post, middle-posterior part of the cingulate gyrus and sulcus; G_front_middle, middle frontal gyrus; G_front_sup, superior frontal gyrus; G_Ins_lg_and_S_cent_ins, long insular gyrus and central sulcus of the insula; G_pariet_inf-Supramar, supramarginal gyrus; G_postcentral, postcentral gyrus; G_rectus, straight gyrus, Gyrus rectus; S_circular_insula_ant, anterior segment of the circular sulcus of the insula; S_front_sup, superior frontal sulcus; S_suborbital, suborbital sulcus; S_temporal_transverse, transverse temporal sulcus; G_insular_short, short insular gyrus; G_parietal_sup, superior parietal lobule; G_precentral, precentral gyrus; G_temp_sup-Plan_tempo, planum temporale or temporal plane of the superior temporal gyrus; G_front_inf-Opercular, opercular part of the inferior frontal gyrus; G_and_S_subcentral, subcentral gyrus (central operculum) and sulci; LH (RH), left (right) hemisphere.

Between-group comparison	Label	Brain regions in LH	*RA* (%)	*p*-Value ($\times 10^{-3}$)	Label	Brain regions in RH	*RA* (%)	*p*-Value ($\times 10^{-3}$)
Post-RT-LD > Pre-RT	R1	G_and_S_cingul-Ant	6.2	5.4	R14	G_and_S_cingul-Ant	7.4	0.8
	R2	G_and_S_cingul-Mid-Ant	6.6	2.2	R15	G_and_S_cingul-Mid-Ant	7.4	1.4
	R3	G_and_S_cingul-Mid-Post	4.4	8.7	R16	G_front_sup	6.0	4.5
	R4	G_front_middle	5.3	3.2	R17	G_insular_short	5.0	1.7
	R5	G_front_sup	6.6	2.4	R18	G_pariet_inf-Supramar	5.6	1.1
	R6	G_Ins_lg_and_S_cent_ins	5.3	8.0	R19	G_parietal_sup	7.9	0.3
	R7	G_pariet_inf-Supramar	4.9	8.8	R20	G_precentral	12.8	0.5
	R8	G_postcentral	6.8	3.6	R21	G_temp_sup-Plan_tempo	6.6	6.1
	R9	G_rectus	5.8	1.2	R22	S_temporal_transverse	10.5	3.4
	R10	S_circular_insula_ant	4.5	8.1	–	–	–	–
	R11	S_front_sup	5.9	4.7	–	–	–	–
	R12	S_suborbital	6.7	6.3	–	–	–	–
	R13	S_temporal_transverse	9.5	3.8	–	–	–	–
Post-RT-LD > Post-RT-ED	R2	G_and_S_cingul-Mid-Ant	10.9	0.1	R15	G_and_S_cingul-Mid-Ant	8.4	2.2
	R3	G_and_S_cingul-Mid-Post	8.3	1.5	R18	G_pariet_inf-Supramar	6.1	0.2
	R7	G_pariet_inf-Supramar	4.9	3.3	R20	G_precentral	12.7	0.6
	R12	S_suborbital	13.9	0.4	R24	G_and_S_subcentral	7.2	1.2
	R23	G_front_inf-Opercular	5.9	2.2	–	–	–	–

compared to the pre-RT group. Fig. 3 shows the locations of these 22 ROIs. For convenient, we referred them as R1 to R22 in the following descriptions. For all these 22 ROIs, we estimated their relative increase rates in cortical thickness and list detail information in Table 3. We found the highest increase rates in three regions, R13 (RA = 9.5%), R20 (RA = 12.8%) and R22 (RA = 10.5%), in the post-RT-LD group compared to the pre-RT group.

3.3.3. Post-RT-ED vs. post-RT-LD

With ROI-wise SBM analysis, we also found uniformly significantly increased cortical thickness in 9 ROIs (R2, R3, R7, R12, R15, R18, R20, R23, and R24) in the post-RT-LD group compared to the post-RT-ED group based on the Destrieux atlas (Fig. 4). Among them, 7 ROIs (R2, R3, R7, R12, R15, R18 and R20) were also found different cortical thickness in *Pre-RT* vs. *post-RT-LD*. In detail, Table 3 lists their relative increase rates in cortical thickness. We found the highest increase rate of cortical thickness in three regions, R2 (*RA* = 10.9%), R12 (*RA* = 13.9%), and R20 (*RA* = 12.7%), in the post-RT-LD group relative to the post-RT-ED group.

For each ROI (R1-R24) listed in Table 3 which showed significant between-group difference in thickness, we assessed the relationship between the cortical thickness and the time after RT, which were shown in Figs. 3 and 4. Bar plots in Figs. 3 and 4 indicated that, for each ROI, the average cortical thickness of the pre-RT group was nearly equal to that of the post-RT-ED group, but the post-RT-LD group had an almost significantly increased average cortical thickness compare to either the pre-RT group or post-RT-ED group.

Fig. 5 plots the *RA* values in cortical thickness of post-RT-ED group vs. pre-RT group, post-RT-LD group vs. pre-RT group, and post-RT-LD group vs. post-RT-ED group, which were obtained according to Eq. (1) and the Destrieux atlas. The positive (negative) *RA* value indicates an increased (decreased) thickness for a given ROI. Fig. 5 shows: 1) compared to the pre-RT, the post-RT-ED had the greatest differences in cortical thickness in the frontal and limbic cortices, 2) compared to the pre-RT, the post-RT-LD had the greatest differences in cortical thickness in the frontal and temporal cortices, and 3) compared to the post-RT-ED, the post-RT-LD had the greatest differences in cortical thickness in the frontal, temporal and limbic cortices.

4. Discussion

Different cortical thickness between the pre-RT, post-RT-ED, and post-RT-LD groups were studied using SBM approaches. We reached the following results: (1) the vertex-wise SBM analysis showed significantly decreased cortical thickness in the post-RT-ED group compared to the pre-RT group at PreCG. And we found that the post-RT-LD group exhibited more profound significantly increased cortical thickness compare to either the pre-RT or post-RT-ED group. Specifically, the post-RT-LD group showed significantly increased cortical thickness in the posterior part of the brain, including the left bSTS, left ICC, left LOC, and bilateral IPC, compared to the pre-RT group. Meanwhile, the post-RT-LD group showed significantly increased cortical thickness in bilateral PreCG compared to the post-RT-ED group. (2) The ROI-wise SBM analysis showed no significant change in cortical thickness in each ROI between the post-RT-ED and pre-RT groups. While the post-RT-LD group exhibited significantly increased cortical thickness in the frontal, temporal, inferior parietal, and cingulate regions compared to either the pre-RT or post-RT-ED group. These findings indicated that radiation-induced alteration of cortical thickness was mainly in the late-delayed period of NPC patients.

4.1. Cortical thickness change little in the post-RT-ED group

With the vertex-wise SBM analysis, we detected that the post-RT-ED group had significantly decreased cortical thickness in only one cluster, the left PreCG which extends across the left postcentral gyrus (PoCG) and left caudal middle frontal cortex (cMFC), compared to the pre-RT group (Fig. 2 and Table 2). The PreCG is a crucial region involving in motor function (Desmurget, et al., 2014; Georgopoulos, 2000). Previous studies (Cheung, et al., 2000; Wang, et al., 2012) indicated that the motor dysfunction was a common symptom in NPC patients after RT. Using VBM method, Lv et al. (2014) found the GM volume deficit in the PreCG in NPC patients after RT, which is consisted with the finding in the present study. The abnormal cortical thickness in the PreCG may be related to the brainstem-RT which has been applied to most patients in the study. As the primary motor pathways originate from the

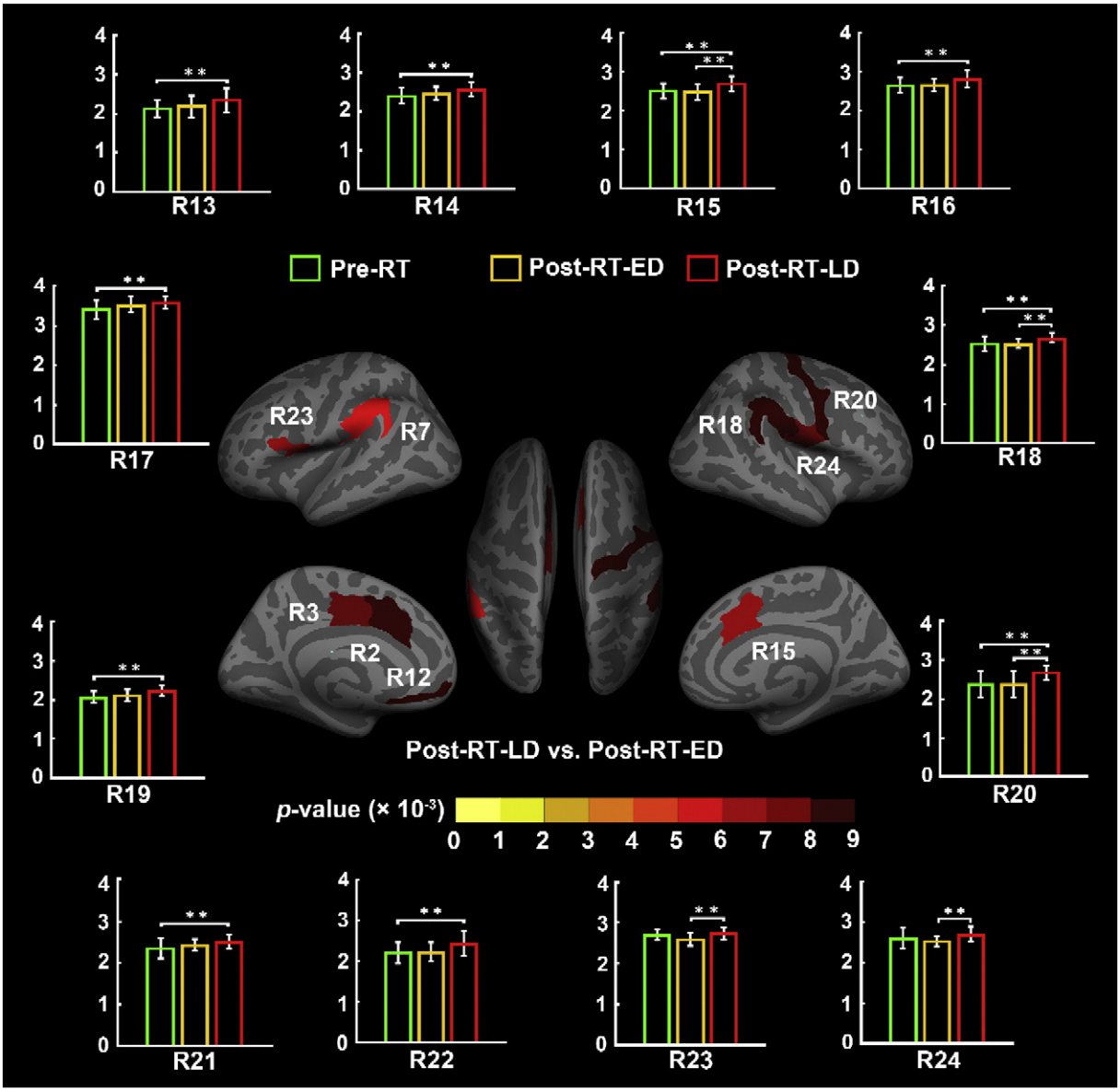

Fig. 4. ROI-wise analysis of cortical thickness between the patients with nasopharyngeal carcinoma in the after radiotherapy (post-RT-ED) group of the early-delayed stage and the after radiotherapy (post-RT-LD) group of the late-delayed stage in this study. This analysis was based on each region of the Destrieux cortical atlas which parcellates each hemisphere into 74 ROIs. Specifically, 9 of the total 148 brain regions in warm color show significantly increased thickness in the post-RT-LD group compared to the post-RT-ED group. Details of cortical thickness for these ROIs are listed in Table 3. In summary, we found 24 ROIs showing significant between-group differences with the ROI-wise analysis. Bar plot of the average cortical thickness for each group in these ROIs are showed in Figs. 3 and 4. The bars and error bars correspond to the average cortical thickness and the standard deviation in the given group. The horizontal cap lines with '**' represent p-value <0.01.

motor cortex and traverse through the brainstem, the irradiation of brainstem might damage the primary motor pathways and then induce the PreCG abnormality (Hua, et al., 2012).

In addition, we also found the post-RT-ED group had decreased cortical thickness in the cMFC and PoCG which are located in the frontal and parietal cortex, compared to the pre-RT group. This result is partially consistent with several previous studies (Duan, et al., 2016; Lv, et al., 2014). Duan et al. (2016) detected lower fractional anisotropy (FA) in the frontal and parietal WM in the post-RT-ED group than that of the pre-RT group. Lv et al. (2014) found GM volume deficit in the parietal cortex in NPC patients after RT. Moreover, previous studies (de Ruiter, et al., 2012; McDonald, et al., 2010) showed that GM volumes in the frontal and parietal lobe changed significantly in breast cancer patients shortly after the chemotherapy completion. Thus, the abnormal cortical thickness of the frontal and parietal cortices in the present study may be related to chemotherapy which has been applied to most NPC patients after RT.

In the post-RT-ED group, we have not found significantly changed cortical thickness in the temporal region, but previous DTI studies (Duan, et al., 2016; Xiong, et al., 2013) have detected abnormal temporal region in the post-RT-ED group. For example, using DTI method, Duan et al. (2016) found higher mean diffusivity in the bilateral temporal regions in the post-RT-ED group than that of the pre-RT group. Xiong et al. (2013) detected lower FA in the temporal region in the post-RT-ED group than that of the pre-RT group. The possible explanation for this discrepancy may be that WM is more sensitive to RT in the early delayed

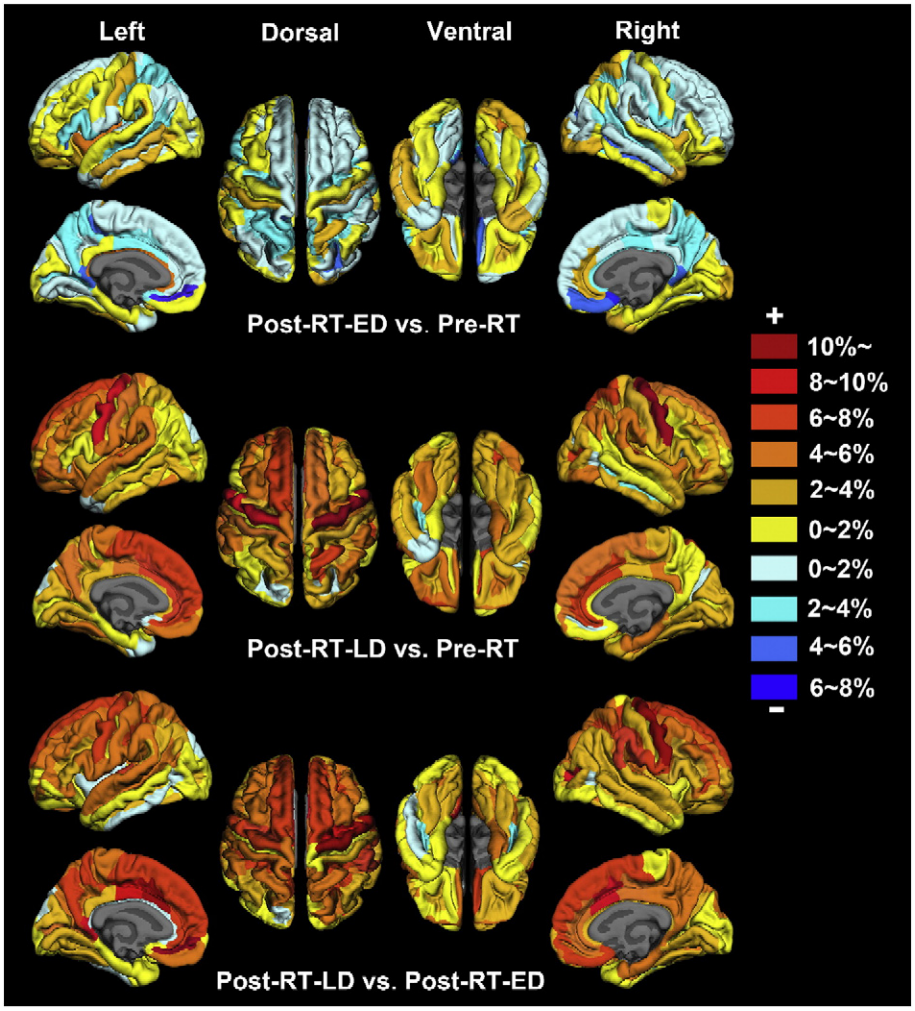

Fig. 5. Radiotherapy-induced relative change of average cortical thickness in the patients with nasopharyngeal carcinoma. The regions coded in cold (warm) color indicate decreased (increased) cortical thickness. The ROI-wise analysis was based on every region of the Destrieux cortical atlas which parcellates each hemisphere into 74 ROIs. The relative alteration of cortical thickness for a given ROI was estimated by $RA_{\text{post-RT-ED}} = (CT_{\text{post-RT-ED}}\text{-}CT_{\text{pre-RT}}) / CT_{\text{pre-RT}}$, $RA_{\text{post-RT-LD}} = (CT_{\text{post-RT-LD}}\text{-}CT_{\text{pre-RT}}) / CT_{\text{pre-RT}}$, $RA_{\text{post-RT-LD}} = (CT_{\text{post-RT-LD}}\text{-}CT_{\text{post-RT-ED}}) / CT_{\text{post-RT-ED}}$, in which RA represents the group relative cortical thickness alteration and $CT_{\text{post-RT-LD}}$ ($CT_{\text{post-RT-ED}}$ or $CT_{\text{pre-RT}}$) represents the group averaged cortical thickness in the post-RT-LD (post-RT-ED or pre-RT) group for a given ROI.

period (Nieman, et al., 2015) and temporal injury may mainly occur in WM in this period. While GM become sensitive to RT and change gradually in the late delayed period.

The ROI-wise SBM analysis revealed that all 148 regions based on the Destrieux atlas did not show significant changes of cortical thickness in the post-RT-ED group compared to pre-RT group.

4.2. Widespread abnormal cortical thickness in the post-RT-LD group

Using vertex-wise SBM analysis, we detected the post-RT-LD group showed significantly increased cortical thickness in widespread areas, including the clusters of the left bSTS, left LOC, left ICC, and bilateral IPC, compared to the pre-RT group, and in the clusters of bilateral PreCG compared to the post-RT-ED group (Fig. 2 and Table 2). These findings indicated that radiation-induced abnormal cortical thickness mainly occur in the post-RT-LD group.

Previous studies (Chan, et al., 1999; Lee, et al., 1988) indicated that radiation-induced brain injury was often found in the temporal region in NPC patients, which is in line with the findings of the present study. The bSTS, a major sulci landmark in the temporal lobe, is considered to be a hub for social perception and cognition, such as the perception of faces (Pitcher, et al., 2011), the understanding others' mental states (Ciaramidaro, et al., 2007), and the performance of language (Fedorenko, et al., 2012). Previous studies showed that NPC patients after RT had damaged social function compared to patients with tumors in other brain regions (Hammerlid, et al., 2001; Leung, et al., 2011). Hsiao et al. (2010) also found that the treated NPC patients had significantly damaged language performance compared to the pre-RT. Thus, the increased cortical thickness in the bSTS may reflect the social and language dysfunctions of the NPC patients in the late-delayed period. Actually, the bSTS, extending to the superior temporal cortex (STC) and middle temporal cortex (MTC) (Fig. 2 and Table 2), received high dose of irradiation in the treatment. Hence, the increased cortical thickness in the bSTS may be mainly attributed to RT.

In this study, we also found significantly increased cortical thickness in the LOC, ICC, and bilateral IPC in the post-RT-LD group compared to the pre-RT group (Fig. 2 and Table 2). The LOC is responsible for the processing of visual shape, object, and face information (Nagy, et al., 2012). Previous studies (Chen, et al., 2005; Fang, et al., 2002) found NPC patients after RT suffered problems of visual processing. The ICC, extending to the precuneus (PreCUN), serves lots of cognitive functions, such as memory (Lim, et al., 2012), emotion (McLaren, et al., 2016), and social function (Doyle-Thomas, et al., 2013). Previous studies (Hsiao, et al., 2010; Tang, et al., 2012) reported memory and emotion dysfunctions in the NPC patients after RT. The IPC is mainly involved in attention, language, episodic memory, and visuo-spatial attention (Cabeza, et al., 2008; Caspers, et al., 2013; Ruschel, et al., 2014). Impairment of language, learning difficulties, and motor dysfunctions were prominent

clinical features in the NPC patients with radiation-induced injury (DeSalvo, 2012; Lell, 2015). Thus, our result indicated RT may have deleterious effects on cognitive functions in NPC patients.

In addition, the ICC, PreCUN, and IPC are core regions associated with the default mode network (DMN) in humans (Buckner, et al., 2008; Greicius, et al., 2003). The dysfunction of DMN was found in various mental disorders, including autism, schizophrenia, and Alzheimer's disease (Buckner, et al., 2008). Our findings of abnormal cortical thickness in these regions indicated that the DMN deficits may have occurred in NPC patients in the late delayed stage, reflecting RT on the brain structure for NPC patients.

The ROI-wise SBM analysis was complementary to the vertex-wise SBM analysis. Both SBM analyses detected increased cortical thickness in the normal-appearing GM in the cingulate, inferior parietal, and the temporal regions in the post-RT-LD group compared to the pre-RT group. However, there were some discrepancies between the results obtained from these two approaches. For example, the abnormal cortical thickness in the frontal and insula regions was detected using the ROI-wise SBM analysis but not found using the vertex-wise SBM analysis. The possible reasons may be related to the process of spatial averaging on cortical thickness estimates in the two SBM analyses (Eyler, et al., 2012). Spatial averaging used in vertex-wise analysis is equivalent to the spatial smoothing, while in the ROI-wise analysis needs to average the cortical thickness across all the vertices within a given region. Moreover, the inter-regional boundaries vary across different subjects which may impact the cortical thickness measurement in the ROI-wise analysis (Li, et al., 2014). In this study, the ROI-wise SBM analysis was used to supplement the findings of vertex-wise SBM analysis.

4.3. Dynamic cortical thickness alterations in the NPC patients

The present study indicated that the alterations of cortical thickness after RT were dynamic and transient in different periods. With vertex-wise SBM analysis, we detected that cortical thickness was significantly decreased in the cluster of PreCG within 6 months after RT (early-delayed stage) compared to pre-RT, then increased to near pre-RT values between 7 and 18 months (late-delayed stage) (Fig. 2 and Table 2). This finding is consistent with a previous DTI study (Xiong, et al., 2013), which indicated that FA in NPC patients after RT were dynamic and transient. Similarly, using the ROI-wise SBM method, we also found the consistent results (Figs. 3-4). Specifically, cortical thickness in the post-RT-ED group showed no significant change compared to the pre-RT group, while cortical thickness was increased significantly in the post-RT-LD group compared to other groups. This finding implies that radiation-induced brain injury for NPC patients might mainly occur in the late-delayed stage.

The cortical thinning is thought to be related to synaptic pruning, a decrease in cell size, neural or glial cell apoptosis and a decrease in spine density (Agostini, et al., 2013; Noble, et al., 2015; Tamnes, et al., 2010). The post-RT-ED group showed significantly decreased cortical thickness in the PreCG compared to the pre-RT group. The possible implication is that the decreased cortical thickness could be related to RT-induced death of neural or glial cell and other abnormal processes initiated by RT or chemotherapy. Previous studies indicated that motor dysfunction was a common symptom in NPC patients after RT (Cheung, et al., 2000; Wang, et al., 2012). Thus, the decreased cortical thickness in the PreCG in the post-RT-ED group may indicate RT-induced motor dysfunction, but the increased cortical thickness in the bSTS, LOC, ICC, and bilateral IPC in the post-RT-LD group may reflect that these regions compensate the impaired functions in the early stage to a certain extent. Actually, the increase of cortical thickness measured with MRI is affected by several factors in the cellular level, such as inflammation and gliosis (Nieman, et al., 2015) or central compensation after particular brain nerve deficits over time (zu Eulenburg, et al., 2010). In addition, it is important to emphasize that the interpretations directly relating macroscopic differences in cortical thickness measured with MRI to differences on the cellular level should be taken with caution.

4.4. Limitations

This study has several limitations. First, the cross-sectional design of this study did not allow us to infer causality between the cortical thickness changes and RT. The reason was that the abnormal cortical thickness in the post-RT-ED and post-RT-LD group could be a pre-existing condition, rather than a consequence of the RT. In the future, a longitudinal study would be better to estimate the effects of RT and time effect on the brain structure in NPC patients. Second, the samples in this study adopted different treatment protocols (2D–CRT and IMRT), which may confound the observed morphometric abnormalities. A previous study indicated greater improvement of treatment results with IMRT than with 2D–CRT (Lai, et al., 2011). It would be better to separate the samples with different treatment protocols in different subgroup in the future study. Third, we have calculated the dose-volume statistics of RT for patients treated under the IMRT protocol. However, the dose-volume statistics of RT for patients under the 2D–CRT treatment was not available due to the technical reasons of the traditional 2D–CRT protocol. Thus, we cannot calculate the relationship between the dose usage of the RT and the alteration of cortical thickness. No doubt, the relationship should be further explored in the future. Fourth, most of NPC patients in this study received chemotherapy in addition to RT, which may confound the generality of the results. Several previous studies indicated that chemotherapy may impact brain structure (de Ruiter, et al., 2012; McDonald, et al., 2010). In the future, we may need to subclass the samples into chemotherapy and RT subgroups for estimating the effect of chemotherapy on cortical thickness in NPC patients. Finally, we did not collect neuropsychological test data and patients' clinical manifestations in this study. Several studies have reported the clinical manifestations of NPC patients after RT and found they exhibited negative emotions, impaired executive, language, and memory abilities (Moretti, et al., 2005; Shen, et al., 2015; Tang, et al., 2012). Moretti et al. (2005) and Shen et al. (2015) also proposed that the dysfunctions in the NPC patients after RT may be related to an underlying neural impairment in the frontal and temporal regions. In the future, we need to make the neurological and cognitive assessments to characterize the clinical manifestations of NPC patients after RT.

5. Conclusion

Using the SBM approach, we estimated the effect of RT on cortical thickness in the NPC patients. The post-RT-ED group showed significantly decreased cortical thickness in the PreCG compared to pre-RT group. And the post-RT-LD group showed significantly increased cortical thickness in widespread brain regions, including the temporal, cingulate, precentral and occipital regions, compared to either the pre-RT or post-RT-ED group. This may imply that RT-induced brain injury for NPC patients mainly occurs in the late-delayed stage and leads to some cognitive dysfunctions. Moreover, the results reflected that RT-induced alterations of cortical thickness were dynamic and transient in different periods. And this finding also suggested that an early intervention is necessary for protecting GM during RT.

Competing interest's statement

The authors declare that they have no competing financial interests.

Acknowledgments

This work was supported by the grants from the Natural Science Foundation of China (Grant Nos. 81401399, 81471654, 81428013, and

81371535), Fundamental Research Funds for the Central Universities (Grant No. 15ykpy35) and Medical Scientific Research Foundation of Guangdong Province (Grant No. B2014162).

References

Agostini, A., Benuzzi, F., Filippini, N., Bertani, A., Scarcelli, A., Farinelli, V., Marchetta, C., Calabrese, C., Rizzello, F., Gionchetti, P., 2013. New insights into the brain involvement in patients with Crohn's disease: a voxel-based morphometry study. Neurogastroenterol. Motil. 25 (147-e82).

Biundo, R., Weis, L., Facchini, S., Formento-Dojot, P., Vallelunga, A., Pilleri, M., Weintraub, D., Antonini, A., 2015. Patterns of cortical thickness associated with impulse control disorders in Parkinson's disease. Mov. Disord. 30, 688–695.

Blanc, F., Colloby, S.J., Philippi, N., de Pétigny, X., Jung, B., Demuynck, C., Phillipps, C., Anthony, P., Thomas, A., Bing, F., 2015. Cortical thickness in dementia with Lewy bodies and Alzheimer's disease: a comparison of prodromal and dementia stages. PLoS One 10, e0127396.

Buckner, R.L., Andrews-Hanna, J.R., Schacter, D.L., 2008. The brain's default network. Ann. N. Y. Acad. Sci. 1124, 1–38.

Cabeza, R., Ciaramelli, E., Olson, I.R., Moscovitch, M., 2008. The parietal cortex and episodic memory: an attentional account. Nat. Rev. Neurosci. 9, 613–625.

Caspers, S., Schleicher, A., Bacha-Trams, M., Palomero-Gallagher, N., Amunts, K., Zilles, K., 2013. Organization of the human inferior parietal lobule based on receptor architectonics. Cereb. Cortex 23, 615–628.

Chan, Y.-L., Leung, S.-F., King, A.D., Choi, P.H., Metreweli, C., 1999. Late radiation injury to the temporal lobes: morphologic evaluation at MR imaging 1. Radiology 213, 800–807.

Chen, P.-R., Hsu, L.-P., Tu, C.-E., Young, Y.-H., 2005. Radiation-induced oscillopsia in nasopharyngeal carcinoma patients. Int. J. Radiat. Oncol. Biol. Phys. 61, 466–470.

Chen, W., Qiu, S., Li, J., Hong, L., Wang, F., Xing, Z., Li, C., 2015. Diffusion tensor imaging study on radiation-induced brain injury in nasopharyngeal carcinoma during and after radiotherapy. Tumori 101, 487–490.

Cheung, M.-C., Chan, A.S., Law, S.C., Chan, J.H., Vincent, K.T., 2000. Cognitive function of patients with nasopharyngeal carcinoma with and without temporal lobe radionecrosis. Arch. Neurol. 57, 1347–1352.

Ciaramidaro, A., Adenzato, M., Enrici, I., Erk, S., Pia, L., Bara, B.G., Walter, H., 2007. The intentional network: how the brain reads varieties of intentions. Neuropsychologia 45, 3105–3113.

Dale, A.M., Fischl, B., Sereno, M.I., 1999. Cortical surface-based analysis: I. Segmentation and surface reconstruction. Neuroimage 9, 179–194.

DeSalvo, M.N., 2012. Radiation necrosis of the pons after radiotherapy for nasopharyngeal carcinoma: diagnosis and treatment. J Radiol Case Rep 6, 9–16.

Desmurget, M., Richard, N., Harquel, S., Baraduc, P., Szathmari, A., Mottolese, C., Sirigu, A., 2014. Neural representations of ethologically relevant hand/mouth synergies in the human precentral gyrus. Proc. Natl. Acad. Sci. U. S. A. 111, 5718–5722.

Destrieux, C., Fischl, B., Dale, A., Halgren, E., 2010. Automatic parcellation of human cortical gyri and sulci using standard anatomical nomenclature. NeuroImage 53, 1–15.

Doyle-Thomas, K.A., Kushki, A., Duerden, E.G., Taylor, M.J., Lerch, J.P., Soorya, L.V., Wang, A.T., Fan, J., Anagnostou, E., 2013. The effect of diagnosis, age, and symptom severity on cortical surface area in the cingulate cortex and insula in autism spectrum disorders. J. Child Neurol. 28, 729–736.

Duan, F., Cheng, J., Jiang, J., Chang, J., Zhang, Y., Qiu, S., 2016. Whole-brain changes in white matter microstructure after radiotherapy for nasopharyngeal carcinoma: a diffusion tensor imaging study. Eur. Arch. Otorhinolaryngol. 273, 4453–4459.

Edge, S.B., Compton, C.C., 2010. The American joint committee on cancer: the 7th edition of the AJCC cancer staging manual and the future of TNM. Ann. Surg. Oncol. 17, 1471–1474.

zu Eulenburg, P., Stoeter, P., Dieterich, M., 2010. Voxel-based morphometry depicts central compensation after vestibular neuritis. Ann. Neurol. 68, 241–249.

Eyler, L.T., Chen, C.-H., Panizzon, M.S., Fennema-Notestine, C., Neale, M.C., Jak, A., Jernigan, T.L., Fischl, B., Franz, C.E., Lyons, M.J., 2012. A comparison of heritability maps of cortical surface area and thickness and the influence of adjustment for whole brain measures: a magnetic resonance imaging twin study. Twin Res Hum Genet 15, 304–314.

Fang, F.-M., Chiu, H.-C., Kuo, W.-R., Wang, C.-J., Leung, S.W., Chen, H.-C., Sun, L.-M., Hsu, H.-C., 2002. Health-related quality of life for nasopharyngeal carcinoma patients with cancer-free survival after treatment. Int. J. Radiat. Oncol. Biol. Phys. 53, 959–968.

Fedorenko, E., Nieto-Castanon, A., Kanwisher, N., 2012. Lexical and syntactic representations in the brain: an fMRI investigation with multi-voxel pattern analyses. Neuropsychologia 50, 499–513.

Fischl, B., Sereno, M.I., Dale, A.M., 1999. Cortical surface-based analysis: II: inflation, flattening, and a surface-based coordinate system. NeuroImage 9, 195–207.

Georgopoulos, A.P., 2000. Neural aspects of cognitive motor control. Curr. Opin. Neurobiol. 10, 238–241.

Giedd, J.N., Rapoport, J.L., 2010. Structural MRI of pediatric brain development: what have we learned and where are we going? Neuron 67, 728–734.

Grant, J.E., Odlaug, B.L., Chamberlain, S.R., 2015. Reduced cortical thickness in gambling disorder: a morphometric MRI study. Eur. Arch. Psychiatry Clin. Neurosci. 265, 655–661.

Greicius, M.D., Krasnow, B., Reiss, A.L., Menon, V., 2003. Functional connectivity in the resting brain: a network analysis of the default mode hypothesis. Proc. Natl. Acad. Sci. U. S. A. 100, 253–258.

Hammerlid, E., Silander, E., Hörnestam, L., Sullivan, M., 2001. Health-related quality of life three years after diagnosis of head and neck cancer—a longitudinal study. Head Neck 23, 113–125.

Hsiao, K.-Y., Yeh, S.-A., Chang, C.-C., Tsai, P.-C., Wu, J.-M., Gau, J.-S., 2010. Cognitive function before and after intensity-modulated radiation therapy in patients with nasopharyngeal carcinoma: a prospective study. Int. J. Radiat. Oncol. Biol. Phys. 77, 722–726.

Hua, C., Merchant, T.E., Gajjar, A., Broniscer, A., Zhang, Y., Li, Y., Glenn, G.R., Kun, L.E., Ogg, R.J., 2012. Brain tumor therapy-induced changes in normal-appearing brainstem measured with longitudinal diffusion tensor imaging. Int. J. Radiat. Oncol. Biol. Phys. 82, 2047–2054.

Jednoróg, K., Altarelli, I., Monzalvo, K., Fluss, J., Dubois, J., Billard, C., Dehaene-Lambertz, G., Ramus, F., 2012. The influence of socioeconomic status on children's brain structure. PLoS One 7, e42486.

Karunamuni, R., Bartsch, H., White, N.S., Moiseenko, V., Carmona, R., Marshall, D.C., Seibert, T.M., McDonald, C.R., Farid, N., Krishnan, A., 2016. Dose-dependent cortical thinning after partial brain irradiation in high-grade glioma. Int. J. Radiat. Oncol. Biol. Phys. 94, 297–304.

Kelly, P.A., Viding, E., Wallace, G.L., Schaer, M., De Brito, S.A., Robustelli, B., McCrory, E.J., 2013. Cortical thickness, surface area, and gyrification abnormalities in children exposed to maltreatment: neural markers of vulnerability? Biol. Psychiatry 74, 845–852.

Khong, P.-L., Leung, L.H.T., Fung, A.S.M., Fong, D.Y.T., Qiu, D., Kwong, D.L.W., Ooi, G.-C., McAlonan, G., Cao, G., Chan, G.C.F., 2006. White matter anisotropy in post-treatment childhood cancer survivors: preliminary evidence of association with neurocognitive function. J. Clin. Oncol. 24, 884–890.

Lai, S.-Z., Li, W.-F., Chen, L., Luo, W., Chen, Y.-Y., Liu, L.-Z., Sun, Y., Lin, A.-H., Liu, M.-Z., Ma, J., 2011. How does intensity-modulated radiotherapy versus conventional two-dimensional radiotherapy influence the treatment results in nasopharyngeal carcinoma patients? Int. J. Radiat. Oncol. Biol. Phys. 80, 661–668.

Lee, A., Ng, S., Ho, J., Tse, V., Poon, Y., Tse, C., Au, G., SK, O., Lau, W., Foo, W., 1988. Clinical diagnosis of late temporal lobe necrosis following radiation therapy for nasopharyngeal carcinoma. Cancer 61, 1535–1542.

Lell, M.M., 2015. Therapy-Induced Changes in Head and Neck. Imaging of Complications and Toxicity following Tumor Therapy. Springer, pp. 95–111.

Leung, S.W., Lee, T.-F., Chien, C.-Y., Chao, P.-J., Tsai, W.-L., Fang, F.-M., 2011. Health-related quality of life in 640 head and neck cancer survivors after radiotherapy using EORTC QLQ-C30 and QLQ-H&N35 questionnaires. BMC Cancer 11, 1.

Li, M., Tian, J., Zhang, R., Qiu, Y., Wen, X., Ma, X., Wang, J., Xu, Y., Jiang, G., Huang, R., 2014. Abnormal cortical thickness in heroin-dependent individuals. NeuroImage 88, 295–307.

Lim, H.K., Jung, W.S., Ahn, K.J., Won, W.Y., Hahn, C., Lee, S.Y., Kim, I., Lee, C.U., 2012. Regional cortical thickness and subcortical volume changes are associated with cognitive impairments in the drug-naive patients with late-onset depression. Neuropsychopharmacology 37, 838–849.

Lv, X.-F., Zheng, X.-L., Zhang, W.-D., Liu, L.-Z., Zhang, Y.-M., Chen, M.-Y., Li, L., 2014. Radiation-induced changes in normal-appearing gray matter in patients with nasopharyngeal carcinoma: a magnetic resonance imaging voxel-based morphometry study. Neuroradiology 56, 423–430.

McDonald, B.C., Conroy, S.K., Ahles, T.A., West, J.D., Saykin, A.J., 2010. Gray matter reduction associated with systemic chemotherapy for breast cancer: a prospective MRI study. Breast Cancer Res. Treat. 123, 819–828.

McLaren, M., Szymkowicz, S., O'Shea, A., Woods, A., Anton, S., Dotson, V., 2016. Dimensions of depressive symptoms and cingulate volumes in older adults. Transl. Psychiatry 6, e788.

Moretti, R., Torre, P., Antonello, R.M., Cattaruzza, T., Cazzato, G., Bava, A., Ukmar, M., Korczyn, A.D., 2005. Neuropsychological evaluation of late-onset post-radiotherapy encephalopathy: a comparison with vascular dementia. J. Neurol. Sci. 229, 195–200.

Nagy, K., Greenlee, M.W., Kovács, G., 2012. The lateral occipital cortex in the face perception network: an effective connectivity study. Front. Psychol. 3, 141.

New, P., 2001. Radiation injury to the nervous system. Curr. Opin. Neurol. 14, 725–734.

Nieman, B.J., de Guzman, A.E., Gazdzinski, L.M., Lerch, J.P., Chakravarty, M.M., Pipitone, J., Strother, D., Fryer, C., Bouffet, E., Laughlin, S., 2015. White and gray matter abnormalities after cranial radiation in children and mice. Int. J. Radiat. Oncol. Biol. Phys. 93, 882–891.

Noble, K.G., Houston, S.M., Brito, N.H., Bartsch, H., Kan, E., Kuperman, J.M., Akshoomoff, N., Amaral, D.G., Bloss, C.S., Libiger, O., 2015. Family income, parental education and brain structure in children and adolescents. Nat. Neurosci. 18, 773–778.

Papmeyer, M., Giles, S., Sussmann, J.E., Kielty, S., Stewart, T., Lawrie, S.M., Whalley, H.C., McIntosh, A.M., 2015. Cortical thickness in individuals at high familial risk of mood disorders as they develop major depressive disorder. Biol. Psychiatry 78, 58–66.

Pereira, J.B., Ibarretxe-Bilbao, N., Marti, M.J., Compta, Y., Junqué, C., Bargallo, N., Tolosa, E., 2012. Assessment of cortical degeneration in patients with Parkinson's disease by voxel-based morphometry, cortical folding, and cortical thickness. Hum. Brain Mapp. 33, 2521–2534.

Peterson, K., Brent Clark, H., Hall, W.A., Truwit, C.L., 1995. Multifocal enhancing magnetic resonance imaging lesions following cranial irradiation. Ann. Neurol. 38, 237–244.

Pitcher, D., Dilks, D.D., Saxe, R.R., Triantafyllou, C., Kanwisher, N., 2011. Differential selectivity for dynamic versus static information in face-selective cortical regions. NeuroImage 56, 2356–2363.

Qiu, L., Lui, S., Kuang, W., Huang, X., Li, J., Zhang, J., Chen, H., Sweeney, J., Gong, Q., 2014. Regional increases of cortical thickness in untreated, first-episode major depressive disorder. Transl. Psychiatry 4, e378.

de Ruiter, M.B., Reneman, L., Boogerd, W., Veltman, D.J., Caan, M., Douaud, G., Lavini, C., Linn, S.C., Boven, E., van Dam, F.S., 2012. Late effects of high-dose adjuvant

chemotherapy on white and gray matter in breast cancer survivors: converging results from multimodal magnetic resonance imaging. Hum. Brain Mapp. 33, 2971–2983.

Ruschel, M., Knösche, T.R., Friederici, A.D., Turner, R., Geyer, S., Anwander, A., 2014. Connectivity architecture and subdivision of the human inferior parietal cortex revealed by diffusion MRI. Cereb. Cortex 24, 2436–2448.

Shen, Q., Lin, F., Rong, X., Yang, W., Li, Y., Cai, Z., Xu, P., Xu, Y., Tang, Y., 2015. Temporal cerebral microbleeds are associated with radiation necrosis and cognitive dysfunction in patients treated for nasopharyngeal carcinoma. Int. J. Radiat. Oncol. Biol. Phys. 94, 1113–1120.

Sun, Y., Zhou, G.-Q., Qi, Z.-Y., Zhang, L., Huang, S.-M., Liu, L.-Z., Li, L., Lin, A.-H., Ma, J., 2013. Radiation-induced temporal lobe injury after intensity modulated radiotherapy in nasopharyngeal carcinoma patients: a dose-volume-outcome analysis. BMC Cancer 13, 397.

Tamnes, C.K., Østby, Y., Fjell, A.M., Westlye, L.T., Due-Tønnessen, P., Walhovd, K.B., 2010. Brain maturation in adolescence and young adulthood: regional age-related changes in cortical thickness and white matter volume and microstructure. Cereb. Cortex 20, 534–548.

Tamnes, C.K., Zeller, B., Amlien, I.K., Kanellopoulos, A., Andersson, S., Due-Tønnessen, P., Ruud, E., Walhovd, K.B., Fjell, A.M., 2015. Cortical surface area and thickness in adult survivors of pediatric acute lymphoblastic leukemia. Pediatr. Blood Cancer 62, 1027–1034.

Tang, Y., Luo, D., Rong, X., Shi, X., Peng, Y., 2012. Psychological disorders, cognitive dysfunction and quality of life in nasopharyngeal carcinoma patients with radiation-induced brain injury. PLoS One 7, e36529.

Wang, H.-Z., Qiu, S.-J., Lv, X.-F., Wang, Y.-Y., Liang, Y., Xiong, W.-F., Ouyang, Z.-B., 2012. Diffusion tensor imaging and 1 H-MRS study on radiation-induced brain injury after nasopharyngeal carcinoma radiotherapy. Clin. Radiol. 67, 340–345.

Xia, P., Fu, K.K., Wong, G.W., Akazawa, C., Verhey, L.J., 2000. Comparison of treatment plans involving intensity-modulated radiotherapy for nasopharyngeal carcinoma. Int. J. Radiat. Oncol. Biol. Phys. 48, 329–337.

Xiong, W.F., Qiu, S.J., Wang, H.Z., Lv, X.F., 2013. 1H-MR spectroscopy and diffusion tensor imaging of normal-appearing temporal white matter in patients with nasopharyngeal carcinoma after irradiation: initial experience. J. Magn. Reson. Imaging 37, 101–108.

Yates, J.W., Chalmer, B., McKegney, F.P., 1980. Evaluation of patients with advanced cancer using the Karnofsky performance status. Cancer 45, 2220–2224.

Zeng, L., Huang, S.-M., Tian, Y.-M., Sun, X.-M., Han, F., Lu, T.-X., Deng, X.-W., 2015. Normal tissue complication probability model for radiation-induced temporal lobe injury after intensity-modulated radiation therapy for nasopharyngeal carcinoma. Radiology 276, 243–249.